Final Draft

of the original manuscript

Krüger-Genge, A.; Hauser, S.; Neffe, A.; Liu, Y.; Lendlein, A.; Pietzsch, J.; Jung, F.:

Response of Endothelial Cells to Gelatin-Based Hydrogels.

In: ACS Biomaterials Science & Engineering. Vol. 7 (2021) 2, 527 - 540.

First published online by ACS: 26.01.2021

https://dx.doi.org/10.1021/acsbiomaterials.0c01432

Response of endothelial cells to gelatin-based hydrogels

Anne Krüger-Genge[1], Sandra Hauser[2], Axel T. Neffe[1,3], Yue Liu[1], Andreas Lendlein[1,3,4], Jens Pietzsch[2,5], Friedrich Jung [1,3*]*

[1] Institute of Active Polymers and Berlin-Brandenburg Centre for Regenerative Therapies (BCRT), Helmholtz-Zentrum Geesthacht, Kantstr. 55, 14513 Teltow, Germany

[2] Helmholtz-Zentrum Dresden-Rossendorf, Institute of Radiopharmaceutical Cancer Research, Department of Radiopharmaceutical and Chemical Biology, Bautzner Landstrasse 400, 01328 Dresden, Germany

[3] Helmholtz Virtual Institute – Multifunctional Biomaterials for Medicine, Kantstr. 55, 14513 Teltow, Germany

[4] Institute of Chemistry, University of Potsdam, Karl-Liebknecht-str. 24-25, 14476 Potsdam, Germany.

[5] Technical University Dresden, School of Science, Faculty of Chemistry and Food Chemistry, 01062 Dresden, Germany

* email: andreas.lendlein@hzg.de, friedrich.jung@hzg.de

KEYWORDS: endothelialization; gelatin-based hydrogel; substrate elasticity; HUVEC function; cell-material-interaction

ABSTRACT

The establishment of confluent endothelial cell (EC) monolayers on implanted materials has been identified as concept to avoid thrombus formation, but is a continuous challenge in cardiovascular device engineering. Here, material properties of gelatin-based hydrogels obtained by reacting gelatin with varying amounts of lysine diisocyanate ethyl ester were correlated with the functional state of hydrogel contacting venous EC (HUVEC) and HUVEC's ability to form a monolayer on these hydrogels.

The density of adherent HUVEC on the softest hydrogel at 37 °C (G' = 1.02 kPa, E = 1.1±0.3 kPa) was significantly lower (125 mm^{-2}) than on the stiffer hydrogels (920 mm^{-2}; G' = 2.515 and 5.02 kPa, E = 4.8±0.8 and 10.3±1.2 kPa). This was accompanied by increased matrix metalloprotease activity (9 $pmol \cdot min^{-1}$ compared to 0.6 $pmol \cdot min^{-1}$) and stress fiber formation, while cell-to-cell contacts were comparable. Likewise, release of eicosanoids (e.g. prostacyclin release of 1.7 vs. 0.2 $pg \cdot mL^{-1} \cdot cell^{-1}$) and the pro-inflammatory cytokine MCP-1 (8 vs. <1.5 $pg \cdot mL^{-1} \cdot cell^{-1}$) was higher on the softer than on the stiffer hydrogels. The expression of pro-inflammatory markers COX-2, COX-1, and RAGE were slightly increased on all hydrogels on day 2 (up to 200% of the control), indicating a weak inflammation, however the levels dropped to below the control from day 6. The study revealed that hydrogels with higher moduli approached the status of a functionally-confluent HUVEC monolayer. The results indicate the promising potential especially of the discussed gelatin-based hydrogels with higher G' as biomaterials for implants foreseen for the venous system.

INTRODUCTION

Vascular endothelial cells (EC) are involved in different tasks. In general, they regulate hemostasis through the expression and secretion of a spectrum of mediators regulating vascular tone and permeability, inflammation, and thrombosis. The luminal surface of quiescent EC, the glycocalyx, is the most blood compatible surface and prevents thrombotic events.[1] Therefore, EC seeding as a means of creating a hemocompatible surface of cardiovascular implants is a strategy to render thrombogenic surfaces hemocompatible.[2] In vivo, the luminal surfaces of cardiovascular devices are often lined only sparsely with endothelial cells.[3-5] Thus, the blood-contacting surface remains unhealed and covered with a layer of compacted plasma proteins only, a so-called pseudointima. Cardiovascular devices therefore can fail, in part due to thrombosis resulting from the lack of endothelium.[6] Moreover, the mismatch in mechanical properties between the elastic native artery and the rigid devices might induce proliferation of vascular smooth muscle cells – leading to hyperplasia and possibly ending up with vascular stenosis/occlusion.[7-8]

Failure of cardiovascular implants can best be avoided by adjusting the elastic modulus of the implant to the surrounding tissue together with the growth of a functionally-confluent monolayer of endothelial cells on the luminal surface. To establish such a cell monolayer on polymer surfaces, optimal adhesion and spreading of the cells is desired.[9] Cell adhesion, migration and proliferation on surfaces are affected by the surface roughness,[10] topography,[11-12] wettability,[13-14] stiffness [15] and chemical composition.[16]

It is reported that EC do not adhere spontaneously to currently available vascular graft materials like expanded polytetrafluoroethylene (ePTFE, Teflon™) and polyethylene terephtalate (PET, Dacron™).[17-18] Furthermore, trans-anastomotic ingrowth of EC in currently used vascular grafts does not exceed 1-2 cm even after years of clinical implantation.[6] Therefore, different strategies were developed to modify polymer surfaces in a way to mimic the natural extracellular matrix (ECM) guiding endothelialization.[19-22] We selected an ECM-based material, gelatin, as it is hydrophilic, provides cell adhesion sites such as RGD and GFOGER peptide sequences[23] and as derivative of collagen forms hydrogels that match tissues in their mechanical and biochemical properties.[24-25] In contrast to collagen which is already used as

implant material, gelatin is not thrombogenic [26] and, does not induce an undesired foreign body reaction upon crosslinking.[27] Stabilization of gelatin-based hydrogels is required to avoid rapid dissolution and may be based on covalent reactions, formation of physical netpoints or supramolecular bonds,[28] or combinations of these.[29] By performing the stabilization step above the helix-to-coil transition temperature of gelatin (~37 °C), the mechanical properties of gelatin-based materials can be tailored through the type and amount of the stabilization reagent. Here, lysine diisocyanate ethyl ester (LDI) was chosen as such reagent, as it is completely derived from a proteinogenic amino acid. The reaction of gelatin and LDI in the presence of water includes several competing reactions.[29] First of all, primary amino groups of gelatin can add to an isocyanate group of LDI forming a urea bond (Figure 1A). Subsequent reaction of a further amino group on another gelatin chain leads to a direct covalent crosslink. However, as the reaction is performed in water, also decarboxylation of isocyanate groups can occur, which may give rise to grafted oligourea groups that may engage in physical interactions as well as to oligourea crosslinks. The stabilization of the gelatin-based system is hence based on physical as well as covalent bonds, and furthermore triple helical gelatin chain regions may be formed acting as further physical netpoints. While the reaction is complex, it is also highly repeatable and gives consistent results over many batches. As nomenclature for the thus produced hydrogels, GX_LNCOY is used, with X being the wt.% gelatin concentration used in the crosslinking, and Y the molar ratio of isocyanate groups of LDI and primary amino groups of gelatin in the reaction. It is known that an increasing ratio Y gives hydrogels with increasing Young's modulus (E = 13±3 kPa (G10_LNCO3), 35±9 kPa (G10_LNCO5) and 55±11 kPa (G10_LNCO8) determined at 37 °C on swollen samples in a water tank.[30]). Figure 1B shows exemplarily the influence of isocyanate:amino group ratio on the hydrogel architecture. In networks formed with higher isocyanate ratio (top) there are more crosslinks, which leads to a denser network with higher Young's modulus and higher density of cellular adhesion sequences than when the hydrogel is formed with lower isocyanate:amino group ratio (bottom). As it is known that cells actively test the mechanical properties of the matrix they grow on (Figure 1C),[31] which leads to changes in gene

transcription by several pathways, in certain elasticity windows a direct effect of material properties on cellular function can be expected (Figure 1D).

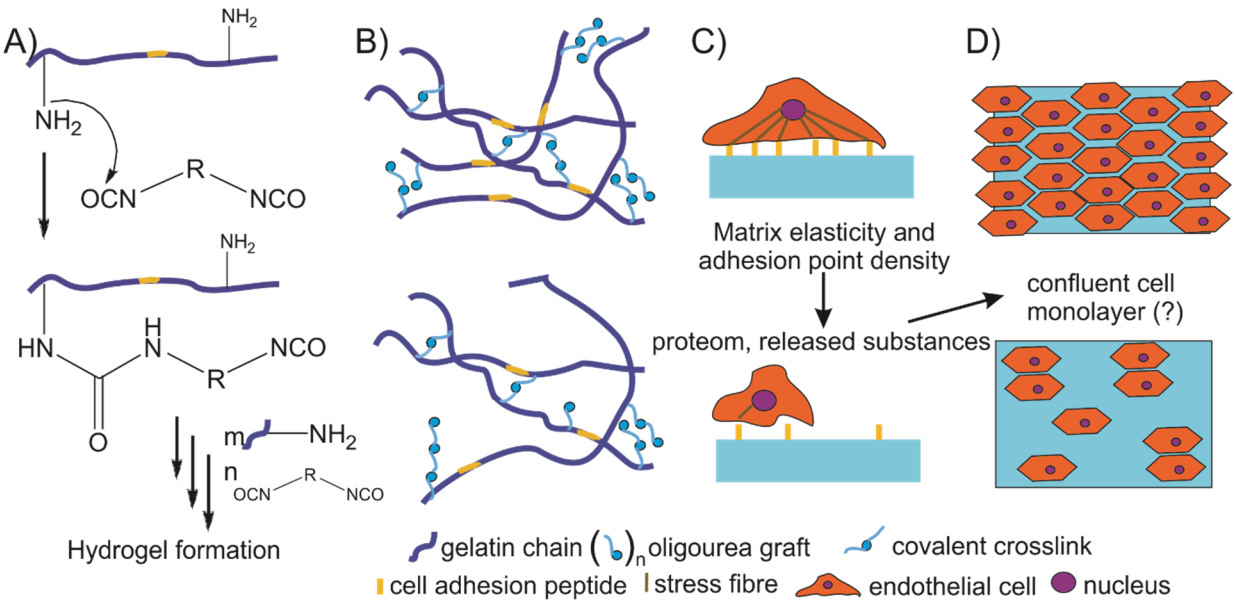

Figure 1. Material synthesis, changes of material properties and their influence on cellular behavior. A) Stabilization of gelatin with lysine diisocyanate occurs through reaction of gelatin primary amino groups with isocyanate groups of LDI, with several competing reactions (see text). B) An increasing amount of LDI in the reaction leads to hydrogels with higher netpoint density, which increases the elastic modulus and the density of cell adhesion sites (top vs. bottom). C) These two properties can be sensed by cells, and via mechanotransduction a change of protein biosynthesis occurs, which leads to changes in cell proteom and release of substances important in cell-cell communication. D) At suitable matrix elasticity and adhesion point density, this might support the formation of a confluent endothelial cell layer.

In addition to the composition dependent hydrolytic[32] and enzymatic degradability in vitro,[33] previous animal studies have shown that these hydrogels degraded in vivo completely without any signs of adverse tissue responses within 35 days (G10_LNCO3) to 84 days (G10_LNCO8).[34-35] Gelatin-based

hydrogels supported the adherence and viability of arterial endothelial cells.[34] However, it is well known that there is significant endothelial cell diversity. EC originating from arteries differ markedly from venous EC in morphology, intercellular junctions, cell surface and growth properties, and in production of basal lamina components.[36] Because the hydrogels are envisioned for devices used in the venous system, this study was performed using human umbilical endothelial cells (HUVEC). We hypothesized that HUVEC can adhere in a vital state, spread and at last establish a functionally-confluent monolayer, with the cellular function depending on the properties of the hydrogel matrix.

In the following, we first describe the physicochemical properties of the investigated hydrogels, including mechanical properties determined by rheology and by AFM, the surface roughness, and the contact angle. Growth of HUVECs on the hydrogels was explored by evaluating the cell density, viability, cell morphology, and the cell-to-cell contacts. Finally, the HUVEC function was explored by quantifying the release of eicosanoids, the activity of released MMPs, as well as the types and amount of cytokines and inflammatory markers.

MATERIALS AND METHODS

Materials

Hydrochloric acid, diethylether, sodium bicarbonate, 2,4,6-trinitrobenzenesulfonic acid (TNBS), poly(ethylene glycol)-*block*-poly(propylene glycol)-*block*-poly(ethylene glycol) (Pluronic® F-108, average M_n ~ 14,600 g·mol^{-1} were purchased from Sigma-Aldrich, Steinheim, Germany. Calcein and rabbit anti-human vWF was from Sigma-Aldrich, Hamburg, Germany. Lysine diisocyanate ethyl ester (LDI) was acquired from CHEMOS, Regenstauf, Germany, and gelatin (from porcine skin, 200 bloom, type A, low endotoxin content) from GELITA USA, Sergeant Bluff, IA, USA. IL-1β, pan-MMP fluorogenic peptide substrate (7-methoxycoumarin-4-yl)acetyl-Pro-Leu-Gly-Leu-(3-[2,4-dinitrophenyl]-l-2,3-diaminopropionyl)-Ala-Arg-NH_2(Mca-Pro-Leu-Gly-Leu-Dpa-Ala-Arg-NH_2 and Recombinant human MMP-9 was bought from R&D Systems, Wiesbaden-Nordenstadt, Germany. Propidium iodide and the solid-phase sandwich VEGF ELISA Kit were purchased from Life Technologies GmbH, Darmstadt, Germany.

Phalloidin-AlexaFluor 488® was fromThermo Fisher Scientific, Darmstadt, Germany, mouse anti-humanVE-cadherin, RIPA lysis buffer (150 mM NaCl, 50 mM Tris pH 8.0, 1% NP40, 0.5 wt.-% SDS, 7 µg/ml leupeptin, 1 mM PMSF, 1 mM Na_3VO_4, 1 mM DTT, 7 mM NaF) and the Prostaglandin E_2 ELISA Kit from Abcam, Cambridge, UK, donkey-anti rabbit DyLight 549 and donkey anti mouse DyLight 488 from Jackson Immuno Research, Hamburg, Germany, 4,6-diamidino-2-phenylindole (DAPI) from Roth, Karlsruhe, Germany), 6-keto Prostaglandin $F_{1\alpha}$ EIA Kit from Cayman Chemicals, Hamburg, Germany , the ELISA kit for Thromboxane A_2 from Cloud-Clone Corp., Cologne, Germany.

Table 1. Antibodies used for Western Blotting

Primary antibodies	**Product Nr.**	**Company**	**Dilution**
anti-COX-2 polyclonal rabbit	PA5-16817	Pierce Biotechnology	1:200
anti-COX-1 polyclonal goat	sc1752	Santa Cruz Biotechnology	1:500
anti-RAGE polyclonal goat	sc8230	Santa Cruz Biotechnology	1:500
anti-ß-actin monoclonal mouse	A5316	Sigma-Aldrich	1:1000
Secondary antibodies	**Product Nr.**	**Company**	**Dilution**
anti-goat IgG POD polyclonal rabbit	A5420	Sigma-Aldrich	1:5000
anti-rabbit IgG POD polyclonal goat	A0545	Sigma-Aldrich	1:2000/1:10000
anti-mouse IgG POD polyclonal rabbit	A9044	Sigma-Aldrich	1:10000

Hydrogel synthesis

Hydrogel films were synthesized as described before[32] by reacting varying amounts of freshly distilled LDI with a 10 wt.-% aqueous gelatin solution, using a 3- (G10_LNCO3), 5- (G10_LNCO5), or 8-fold (G10_LNCO8) excess of isocyanate groups compared to amino groups of gelatin. The quantification was performed using a TNBS assay [37]. The reaction was performed in the presence of 1 wt.-% Pluronic® F-108. Samples were sterilized by ethylene oxide sterilization (gas phase: 6 vol.-% ethylene oxide, 45 °C, 65% relative humidity, 1.7 bar, gas exposure time: 3 h, aeration phase: 12 h) using a DMB-SteriVIT-Automatik Typ 100 VS 12 (DMB-Apparatebau, Wörrstadt, Germany).

Rheological Measurements

The rheological behavior of hydrogel networks swollen to equilibrium in deionized water was investigated on a HAAKE MARS III rheometer (Thermo Fischer Scientific, Reichenthal, Germany) using samples of 20 mm diameter in a 20 mm plate-plate measurement geometry with Peltier element for temperature control. Measurements were performed at room temperature under constant shear stress of 4 Pa and a constant oscillation frequency of 1 Hz for 180 s, which corresponded to the linear viscoelastic region as determined prior. Evaporation of water and drying of samples during the temperature sweep was reduced by covering the sensor plates with a Teflon solvent trap and using a solvent reservoir. The storage modulus was determined at 37 °C and the mesh size as calculated according to equation 1 [38]:

$$\xi = \left(\frac{RT}{G' N}\right)^{1/3} \qquad \text{(equation 1)}$$

where G´ is the storage modulus, N the Avogadro constant, R the molar gas constant and T the temperature [15].

Contact angle measurements

Dynamic contact angle (DCA) measurements were conducted in ultra-pure deionised water with a conductivity of 0.050 µS/cm (Ultra Clear UV clean water system, SG Wasseraufbereitung und Regenerierstation GmbH, Barsbüttel, Germany) at ambient temperature on a drop shape analyzer (DSA 100, Krüss GmbH, Hamburg, Germany) using the captive bubble method. Advancing and receding contact angle measurements were performed by stepwise withdrawing/adding of air from/to the captured bubble, while the bubble was increased with each measurement cycle from 2 to 5 mm in diameter. Prior to the DCA measurement, all samples were preconditioned for 24 hours in deionised water at ambient temperature for equilibration. At least five measurements for advancing and receding

angles on three different locations were performed for each sample. The average of the contact angles was calculated as well as the standard deviation.

Atomic force microscopy

Surface topography investigations and local mechanical analysis of the polymeric substrates were performed by AC-mode scanning and nanoindentation using an atomic force microscope (MFP-3D, Asylum Research, Santa Barbara, USA). A bio Petri dish holder (Asylum Research, Santa Barbara, USA) was utilized as sample holder, enabling measurements in deionized water at ambient temperature. The hydrogel samples were fixed to the bottom of petri dish using Second Glue (UHU, Buehl, Germany) during hydrated state. Before measurements, the AFM components such as the cantilever spring constant and piezoelectric scanner movement were calibrated based on a clean silicon wafer in air and water, while the samples were immersed and equilibrated in deionized water at room temperature for 1 hour.

AC-mode scanning was conducted with TR400PB gold coated silicon nitride cantilevers (Asylum Research, Santa Barbara, USA) having a typical spring constant of 0.09 $N \cdot m^{-1}$ at a scan size of 10 x 10 µm with a scan rate of 0.2 Hz. For each sample scans on three different locations were scanned and the root-mean-square roughness (R_q) of each image was calculated by the software AR15.09.112 based on Igor Pro 6.37A (WaveMetrics, Inc., Portland, OR, USA).

Nanoindentation measurements were performed with cantilevers (TR400PB, Asylum Research, Santa Barbara, USA) having a spring constant of 0.095 $N \cdot m^{-1}$ for hydrogel samples and the applied indentation force F was 10 nN. Based on 15 single indentations performed on different locations of each sample and average values for the indentation depth (δ) and the reduced Young's moduli (E) were analyzed. E was calculated from the force-distance curves according to the Oliver-Pharr model for G10_LNCO3 and the Hertz model for G10_LNCO5 and G10_LNCO8 by the software AR15.09.112 based on Igor Pro 6.37A (WaveMetrics, Inc., Portland, OR, USA) .

Study design

The formation of an endothelial cell monolayer on three gelatin-based hydrogels - differing in their mechanical properties - was evaluated using human umbilical venous endothelial cells (HUVEC). A time period of nine days was considered to be sufficient to form functional confluence [39]. The HUVEC monolayer was investigated after two, six and nine days of cultivation with the assessment of cell density, viability, morphology, cell-to-cell and cell-to-substrate interactions and the cell function including pro-inflammatory markers. The cultivation of HUVEC on glass is named in the following as "untreated control", while the addition of IL-1β to HUVEC seeded on glass will be named as "pro-inflammatory treated control (ITC)".

Endothelial cells

Primary human umbilical venous endothelial cells (HUVEC; Lonza, Cologne, Germany) of the 4th passage [40] were cultured in EGM-2 under static cell culture conditions (37 °C, 5% humidity). 50,000 HUVEC per well (24-well plate, TPP, Trasadingen, Switzerland) were seeded on the three hydrogels (n=7), swollen overnight in cell culture medium. As untreated control, HUVEC were cultivated in pure culture medium on glass as standard substrate (Gerhard Menzel GmbH, Braunschweig, Germany). Additionally, HUVEC were analyzed under pro-inflammatory conditions (seeded on glass in EGM-2 supplemented with 10 ng/ml IL-1β). The experiments including cell density analysis, viability analysis, immunocytochemistry, analyses of released HUVEC mediators, and protein expression were performed at day 2, 6, and 9 after cell seeding.

Cell density and viability analysis

To investigate the number of adherent live and dead cells a calcein/propidium iodide staining was performed. Briefly, 2 µM calcein, which stains viable cells in green, was added to the HUVEC and incubated at 37 °C for 45 min. Subsequently, 2 µM propidium iodide, which stains dead cells in red, was added and 3 positions per well were examined using a confocal laser scanning microscope (LSM 510 META, Zeiss, Oberkochen).

Immunocytochemistry

Cell morphology, actin filaments, cell-to-cell contacts and endothelial cell marker were visualized after paraformaldehyde fixation of the HUVEC as described in [41]. Cells were fixed at room temperature using 4 wt-% paraformaldehyde with subsequent permeabilization using Triton X-100 (0.5 wt-%). F-actin was stained using phalloidin-AlexaFluor 488® (Thermo Fisher Scientific, Darmstadt, Germany). VE-cadherin and von-Willebrand-factor (vWF) were visualized applying rabbit anti-human vWF and mouse anti-humanVE-cadherin as primary antibodies. As secondary antibodies donkey-anti rabbit DyLight 549 and donkey anti mouse DyLight 488 were used. Nuclei were visualized with 4,6-diamidino-2-phenylindole.

Analysis of Eicosanoids

The concentration of prostacyclin was measured in the supernatant of HUVEC using the 6-keto Prostaglandin $F_{1\alpha}$ EIA Kit, of prostaglandin E_2 using an *in vitro* competitive ELISA assay according to the manufacturer´s instructions, and of TXA_2 using the ELISA kit for Thromboxane A_2. All analyses were performed according to the manufacturer´s instruction.

Analysis of cytokines

The secretion of cytokines in the supernatant of HUVEC was quantified using a Multiplex System (Bioplex200®, Bio-Rad München, Germany) with Bio-plex Pro Human Cytokine27-plex from Bio-Rad.

The concentration of VEGF was measured in the supernatant of HUVEC using a solid-phase sandwich VEGF ELISA Kit. All analyses were performed according to the manufacturer´s instruction.

Analysis of MMP activity

The MMP activity was determined in the cell culture supernatant of HUVEC applying the pan-MMP fluorogenic peptide substrate (7-methoxycoumarin-4-yl)acetyl-Pro-Leu-Gly-Leu-(3-[2,4-dinitrophenyl]-l-

2,3-diaminopropionyl)-Ala-Arg-NH_2(Mca-Pro-Leu-Gly-Leu-Dpa-Ala-Arg-NH_2. Recombinant human MMP-9 served as positive control. The analysis was performed as described [42].

Protein expression

In order to determine the effect of substrate contact on the protein synthesis, HUVEC were cultivated on the hydrogels in 6-well plates (1×10^6 cells/well in 5 ml medium) for 2, 6 and 9 days. Cells were detached using a 2 mM EDTA in PBS solution for 30 min and centrifuged at 300 × g for 5 min, and the cell pellet was collected in 100 µl RIPA lysis buffer. After cell lysis, SDS-PAGE using 50 µg protein/lane and Western blotting were performed as described previously [34, 43]. Western Blots were incubated with primary and secondary antibodies as shown in Table 1. Images of Western Blots were evaluated using densitometric analysis [34].

Densitometry

Densitometrical analysis was performed via 1D gel analysis software Total Lab with a minimum profile background subtraction and automatic band detection (minimum slope 350, noise reduction 5%, 3% of maximum peak). The resulting values for the area under the curve (AUC) were used to calculate the densitometric index for each protein of interest ($DI_{protein\ of\ interest}$) for each sample using equation 2) [34, 43].

$$DI_{protein\ of\ interest} = \frac{AUC_{protein\ of\ interest}}{AUC_{\beta-actin}} \qquad \text{(Equation 2)}$$

In order to calculate the relative expression, the value of each sample's $DI_{protein\ of\ interest}$ was related to the $DI_{protein\ of\ interest}$ of the medium sample of the same experiment and day, which was set to 100%. Percentage values of all experiments were used for statistical analysis.

Statistical analysis

Descriptive data were expressed as arithmetic mean ± standard deviation (SD), and statistical significance was evaluated by one-way or when appropriate two-way ANOVA coupled with a *post hoc*

Bonferroni correction analysis using Graph Pad Prism software. *P* values below 0.05 are considered significant.

RESULTS

Physicochemical characterization of the films

The synthesis process of the films did not allow to use one batch of materials for all characterizations and biological evaluations. Therefore, we established the stability of the process by cross-batch comparison of the rheological behavior and water uptake of samples synthesized over a longer period of time (>1 year), and using these methods also for quality control. All physicochemical tests reported here were performed after sterilization. The water uptake of the samples at 37 °C was highest for G10_LNCO3 (1100±190 wt.%), and similar for the other two hydrogel compositions (G10_LNCO5: 710±35 wt.%, G10_LNCO8: 720±55 wt.%). Quality control furthermore consisted of FT-IR measurements verifying the complete conversion of the isocyanate groups. Figure 2 shows the FT-IR spectra of gelatin, LDI, and the three hydrogels.

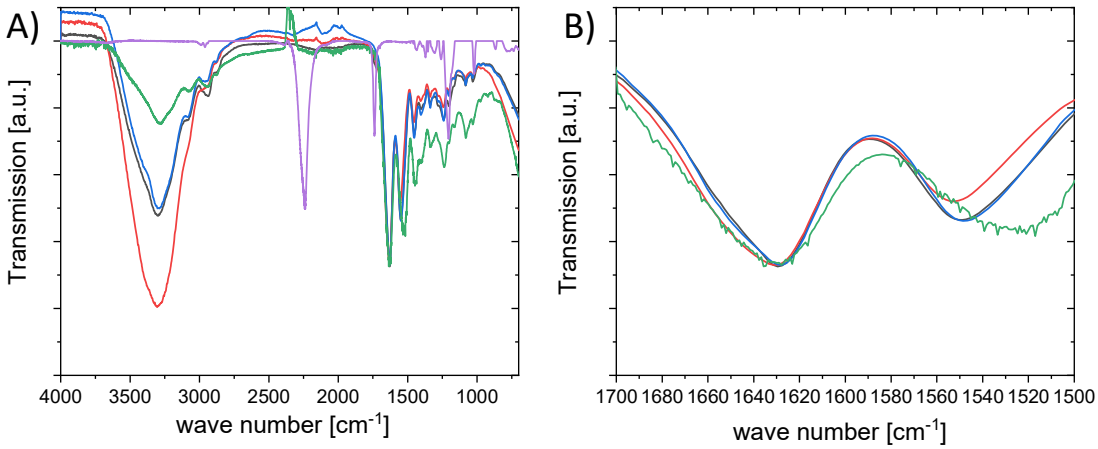

Figure 2. IR spectra of gelatin (green), LDI (purple) and the films G10_LNCO3 (black), G10_LNCO5 (red), and G10_LNCO8 (blue). A) Full spectrum, B) excerpt (LDI not displayed). The spectra have been normalized to the peak intensity at ~ 1627 cm^{-1} for comparison.

An isocyanate band occurs in IR spectra at 2200-2250 cm^{-1}, and can be prominently seen in the spectrum of LDI (Figure 2A). This band is not observed in the hydrogels. All other bands are alike for the starting material and the hydrogels, indicating that the materials are proteinaceous, which means that typical functional groups present on the surface and within the material are corresponding to the composition of gelatin and include in particular amides, carboxylic acids, alcohols and amino groups. Figure 2B shows an excerpt of the Amide I/Amide II region of the spectra. (LDI not displayed). The amide I band occurred at 1627 cm^{-1} for gelatin and the investigated dried hydrogels, while the amide II bond was observed at 1547-1552 cm^{-1} for the networks and at 1524 cm^{-1} for gelatin.

The storage modulus G' and complex viscosities η^* of the hydrogels determined by rheology increased with rising LDI amount and therefore correlated with each other. Representative depictions of time sweep rheological studies of the hydrogels showing the G', the loss moduli G'' and $\eta^*$are shown in Supporting Information Figure S1. At all time points, the storage moduli of the hydrogels was higher than the corresponding loss moduli. G' values reported in Table 2 are middled over several batches. The mesh size ξ, calculated from the measured storage modulus showed a decrease with increasing G'. The reduced elasticity modulus E_{red} determined by AFM (and the Young's modulus E calculated from the experiment) likewise increased continuously with increasing molar ratios of lysin diisocyanate ethyl ester ($p<0.01$) and at the same time the indentation depth (I_d) decreased ($p<0.01$).

Table 2. Physicochemical properties of gelatin-based hydrogels

Property	G10_LNCO3	G10_LNCO5	G10_LNCO8
G' [kPa][a,b]	1.02±0.72	2.515±0.56	5.025±1.65
ξ [nm][a,b]	16±4	12±1	9±1
E_{red} [kPa][c,d,e]	1.2±0.3	6.6±1.2	14.3±1.6
I_d [µm][c,d,e]	3.1±0.5	1.9±0.2	1.1±0.1

E [kPa][c,d,e,f]		1.1±0.3	4.8±0.8	10.3±1.2
R_a [nm][c,e]		11.6±9.2	66.3±15.7	32.1±4.4
R_q [nm][c,e]		15.3±12.4	83.1±21.9	41.6±4.5
Contact angle [°][c,e]	Adv.	67.8±6.4	56.9±3.8	70.2±4.6
	Rec.	36.2±8.8	26.1±7.0	34.6±4.2
	Hys.	31.6	30.8	35.6

[a] at 37 °C, [b] sample size ≥7, [c] at ambient temperature, [d] sample size: n=15, [e] in ultra-pure deionized water, [f] calculated from the indentation experiments. Adv.: advancing; Rec.: receding; Hys: hysteresis.

Atomic force microscopy was furthermore employed to determine the surface roughness of the swollen samples in deionized water at ambient temperature (Table 2) The surface roughness of the three hydrogels differed significantly ($p<0.05$), with the highest values found for G10_LNCO5. The contact angles determined in a dynamic assay also differed ($p<0.05$). Here, the highest values were found for G10_LNCO8.

Cell density of HUVEC on gelatin-based hydrogels

To determine the influence of structural differences in the set of hydrogels on the HUVEC attachment, the density of adherent HUVEC per mm^2 was quantified (Figure 3). On the second day of cultivation significantly less HUVEC adhered to the three gelatin-based hydrogels compared to both controls on glass (+/- IL-1β, $p<0.001$ each). Subsequently, the numbers of adherent HUVEC on G10_LNCO5 and G10_LNCO8 significantly increased until the ninth day of cultivation ($p<0.001$ each), but remained below the density of adherent HUVEC on glass, while they were higher compared to the IL-1β control.

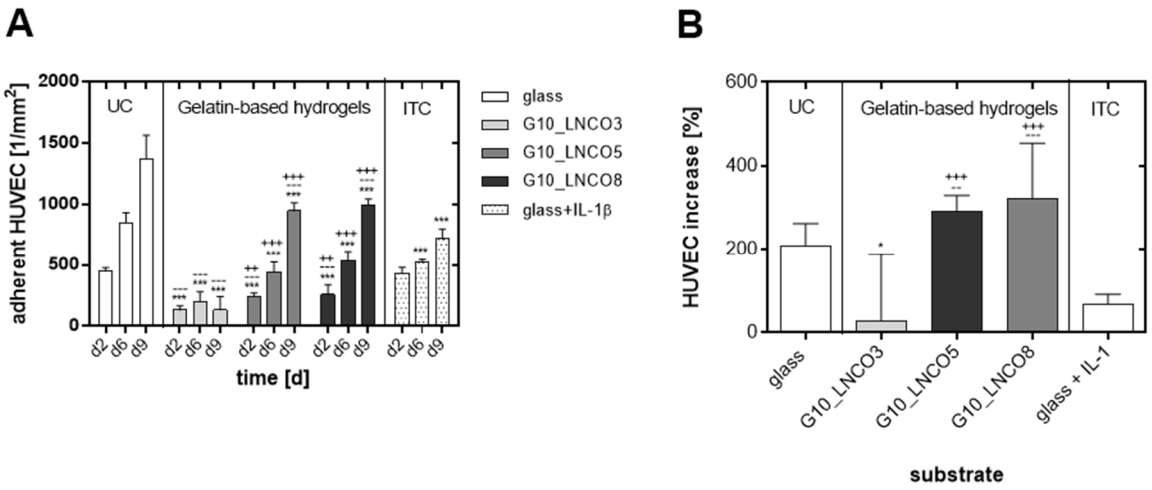

Figure 3. (A) Number of adherent HUVEC per mm^2 on the three hydrogels in comparison to glass as well as to the IL-1β-treated control after 2, 6 and 9 days of cultivation. The number of adherent HUVEC was determined by confocal laser scanning microscopy after calcein and propidium iodide staining. Arithmetic mean ± SD of n=7 experiments is shown. (B): Increase of adherent HUVEC from day 2 to day 9 of cultivation for the three hydrogels in comparison to glass as untreated control (UC) as well as to the IL-1β-treated control (ITC). *: $p < 0.05$ versus glass, ***: $p < 0.001$ versus glass, ++: $p < 0.01$ versus G10_LNCO3, +++: $p < 0.001$ versus G10_LNCO3, --: $p < 0.01$ versus IL-1β, ---: $p < 0.001$ versus IL-1β.

However, the numbers of adherent HUVEC on G10_LNCO5 (291±38%) and G10_LNCO8 (321±133%) increased faster than on both controls after the second day (209±53% or 67±24% respectively). Completely different results were found on G10_LNCO3, where the number of adherent HUVEC remained unchanged over time.

Supplementation of culture medium with IL-1β led to a reduction of adherent HUVEC. Here the density of adherent HUVEC was lower than on glass and on G10_LNCO5 ($p<0.01$) or on G10_LNCO8 ($p<0.001$).

Viability of HUVEC on gelatin-based hydrogels

The percentage of viable adherent HUVEC on the three hydrogels was comparable to the percentage of viable adherent HUVEC on glass over the complete cultivation time (Figure S2). Cultivation on

G10_LNCO8, particularly, resulted in a higher viability than on the IL-1β treated control after two ($p<0.01$) and six ($p<0.001$) days of cell cultivation.

Figure S3 shows the typical pattern of calcein/propidium iodide-stained HUVEC on the different materials nine days after seeding. On all surfaces the majority of HUVEC were viable.

Cell morphology and cell-to-cell contacts of HUVEC on gelatin-based hydrogels

For the formation of a functionally-confluent HUVEC monolayer, which is of vital importance for the non-thrombogenicity of cardiovascular devices, the morphology of adherent HUVEC and the formation of cell-to-substrate as well as of cell-to-cell contacts (Figure 4) is essential. Only on glass an optically nearly confluent HUVEC layer was formed after nine days of cultivation. A substantial number of cells were in a round and non-spread state but not in conjunction with the neighboring cells. The addition of IL-1β to the culture medium led to a completely different pattern with much larger and spindle-shaped cells. Here, significantly less HUVEC adhered remaining in a very active and migrating state.

The behavior of HUVEC on the three hydrogels clearly differed beyond the density of adherent cells. For all time points stress fibers could be observed in central parts of HUVEC seeded on the hydrogels (most pronounced on G10_LNCO3, Figure 4). However, stress fibers decreased with cultivation time, at the same time developing a marginal filament band (least pronounced on G10_LNCO3) supporting and stabilizing cellular adherence. It was particularly striking that HUVEC adhering to G10_LNCO3 were also spindle shaped comparable to HUVEC after adding IL-1β mimicking a pro-inflammatory driven situation. They appeared activated, were migrating, and showed a maximum of stress fibers in central parts of the cells – in contrast to the other hydrogels (Figure 4) over the whole cultivation period. On G10_LNCO5 and G10_LNCO8, HUVEC were mostly in a spread status partially forming a monolayer. On all hydrogels, islands without HUVEC were visible. These holes in the HUVEC layers were found in larger cavities at the surface of the hydrogels where no cells had grown into, while smaller cavities were filled out by HUVEC.

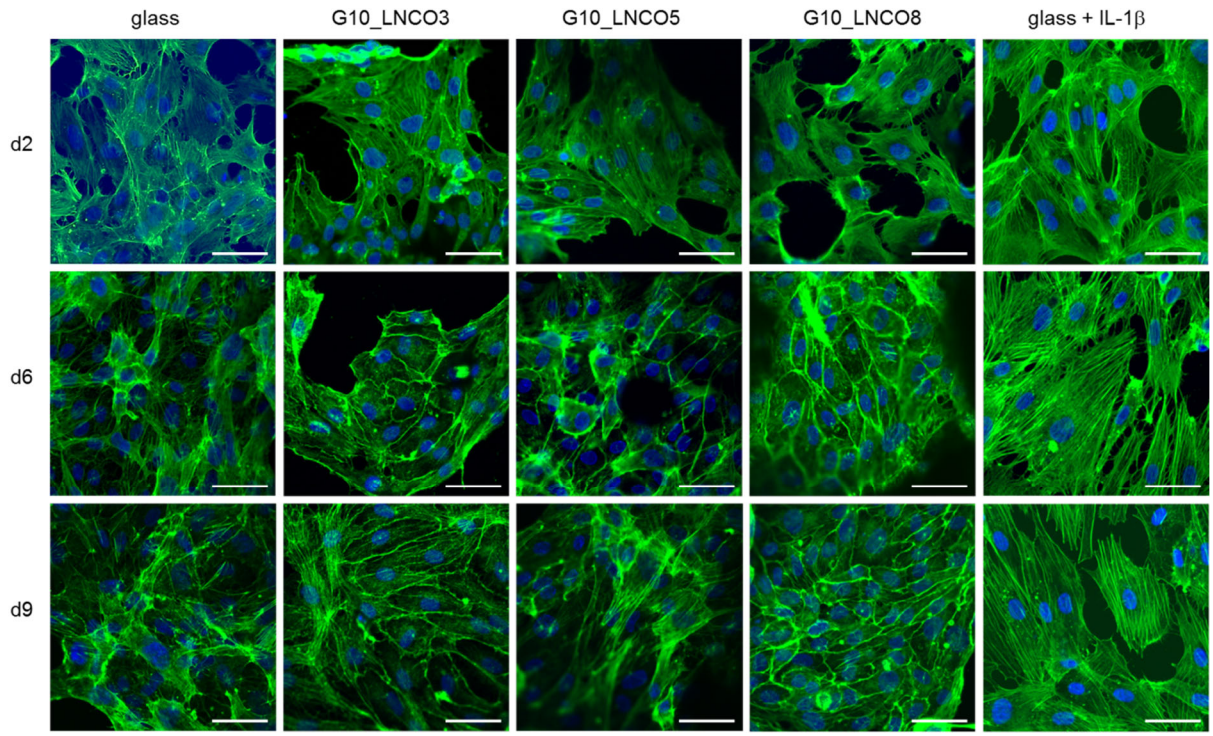

Figure 4. Stress fiber formation in HUVEC on the three hydrogels in comparison to glass as well as to the IL-1β-treated control after 2, 6 and 9 days of cultivation. F-actin is stained in green nuclei in blue using DAPI and images were acquired by confocal laser scanning microscopy. Images are presented in 63x primary magnification. Scale bar: 50 µm

Already at day six and even more pronounced at day nine, the stress fiber formation was declining on G10_LNCO5 demonstrating a good cell-to-cell and cell-to-substrate binding. This was also - but less pronounced - the case on G10_LNCO8 and in only some cells on G10_LNCO3. A massive stress fiber formation still occurred at day 9 on glass and in the IL-1β-supplemented cultures.

Transmembranous VE-Cadherin glycoproteins are parts of cell-to-cell adhesion receptors, localized in adherent junctions of EC, associated with the actin-containing cytoskeleton [44] and mediate the intercellular adhesion necessary for the EC monolayer integrity [45]. VE-Cadherin was expressed similarly in HUVEC seeded on the different gelatin-based hydrogels and on glass (Figure 5). Already at day six, interdigitating cadherins demonstrate the good cell-to-cell binding especially on G10_LNCO5 and a bit

less also on G10_LNCO8. HUVEC treated with IL-1 β obviously exhibited an inhomogeneous, discontinuous expression of this cell membrane glycoprotein in the cell rim combined with a clustering in the basal part of the cell.

HUVEC especially on G10_LNCO5 showed signs of early maturation at day six (von-Willebrand-Factor (vWF) and the formation of first Weibel Palade bodies). This also occurred on G10_LNCO8 at day nine (Figure 5).

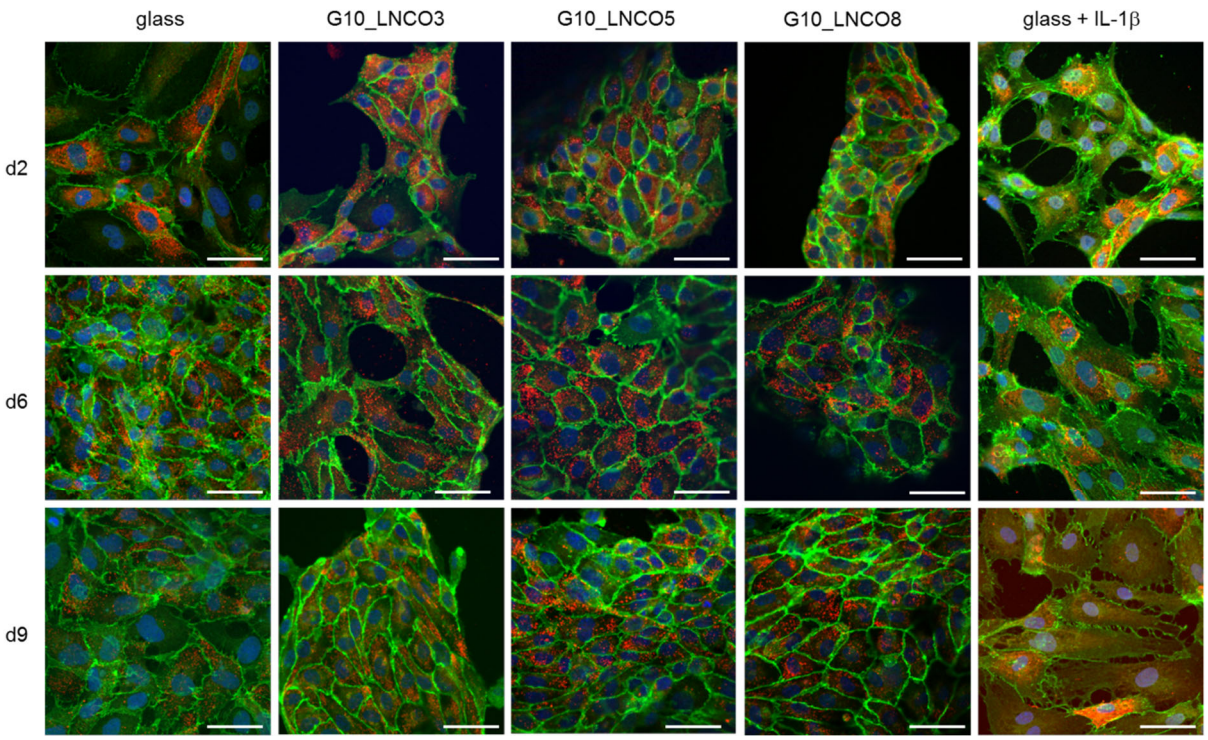

Figure 5. VE-Cadherin and vWF expression in HUVEC seeded on the three hydrogels in comparison to glass as untreated control as well as to the IL-1β-treated control after 2, 6 and 9 days of cultivation. Cell membrane associated VE-Cadherin is stained in green, vWF in red, nuclei in blue using DAPI and images were acquired by confocal laser scanning microscopy. Images are presented in 63x primary magnification. Scale bar: 50 µm

Analysis of HUVEC function on gelatin-based hydrogels

I. Secretion of eicosanoids (prostacyclin, thromboxane A_2, prostaglandin E_2)

The release of prostacyclin (PGI_2), a marker of HUVEC function involved in the regulation of the vascular tone, in pro-inflammatory and anti-thrombogenic processes *in vivo*, was similar from HUVEC seeded on the three hydrogels and comparable to both controls at day two and six of cultivation. In contrast, at day nine of cultivation the highest release was seen from HUVEC cultivated on G10_LNCO3 compared to G10_LNCO5, G10_LNCO8, and glass ($p<0.001$ each) as well as compared to the IL-1β-treated control ($p<0.01$) (Figure 6).

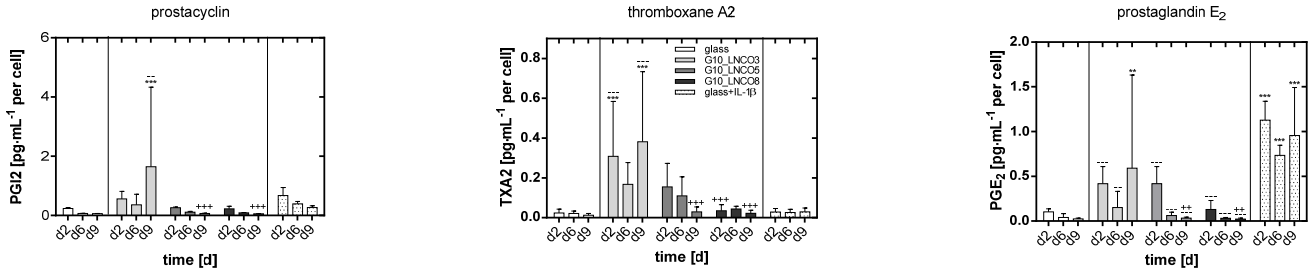

Figure 6. (A) Prostacyclin concentration (PGI_2 in [pg·mL^{-1} per cell]), (B) thromboxane A_2 concentration (TXA_2 in [pg·mL^{-1} per cell]), and (C) prostaglandin E_2 concentration (PGE_2 in [pg·mL^{-1} per cell]) in cell culture supernatants of HUVEC seeded on the three hydrogels in comparison to glass as well as to the IL-1β-treated control (ITC) after 2, 6 and 9 days of cultivation. Arithmetic mean ± SD of n=7 experiments is shown. Statistical analysis was performed using Two-way ANOVA and Bonferroni post hoc test.**: $p < 0.01$ versus glass, ***: $p < 0.001$ versus glass, ++: $p < 0.01$ versus G10_LNCO3, +++: $p < 0.001$ versus G10_LNCO3, --: $p < 0.01$ versus IL-1β, ---: $p < 0.001$ versus IL-1β

II. Activity of secreted matrix metalloproteases

The activity of various secreted matrix metalloproteases (MMPs) - which are involved in the degradation of ECM and biomaterials - was significantly increased at day two and nine of cultivation for HUVEC seeded on G10_LNCO3 compared to G10_LNCO5, G10_LNCO8 and both controls ($p<0.001$, each). The MMP activity of HUVEC grown on G10_LNCO5 and G10_LNCO8 was comparable at day six and day nine of cell growth (Figure 7).

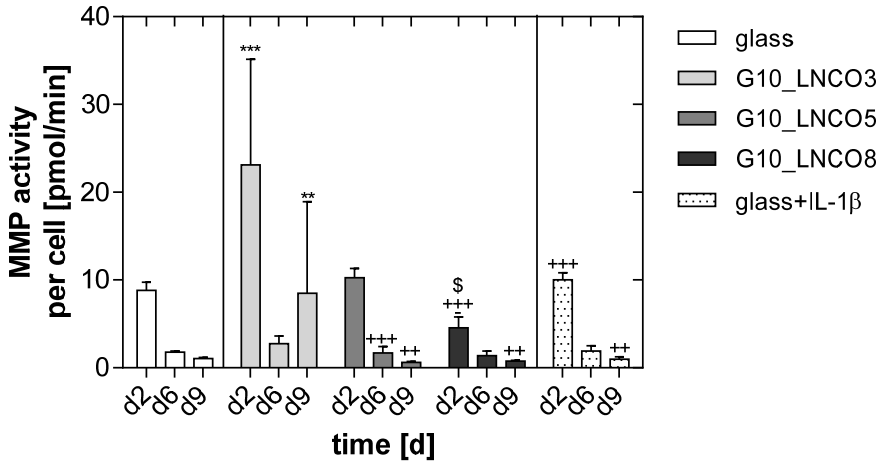

Figure 7. MMP activity in the cell culture supernatant of HUVEC seeded on the three hydrogels in comparison to glass as well as to the IL-1β-treated control after 2, 6 and 9 days of cell cultivation. The MMP activity was analyzed by the cleavage of a fluorogenic MMP specific substrate leading to an increase of fluorescence intensity. MMP activity of n=7 is given by the arithmetic mean ± standard deviation of pmol substrate·min^{-1}. Statistical analysis was performed using Two-way ANOVA and Bonferroni post hoc test. ** : $p < 0.01$ versus glass, ++ :$p < 0.01$ versus G10_LNCO3, +++: $p < 0.001$ versus G10_LNCO3, $: $p < 0.05$ versus G10_LNCO5.

III. Analysis of HUVEC cytokines

Cytokines comprise a large family of proteins, which affect the interaction and communication of cells directing the integration or rejection of an implanted device. Further on, they can act pro-angiogenic. A broad range of cytokines was measured in the supernatants of HUVEC at days two, six and nine of cultivation on the gelatin-based biomaterials (Figure 8).

PDGF-BB did not differ for the three hydrogels after two and six days of HUVEC cultivation, but was increased to the level of the IL-1β-treated control on G10_LNCO3 compared to both other hydrogels ($p<0.001$ each) and also compared to glass ($p<0.001$) at day nine. HUVEC treated with IL-1β showed a similar release of PDGF-BB as the three hydrogels on day two, but the release was significantly higher at days six and nine ($p<0.01$ each).

Significant higher concentrations of VEGF were released by HUVEC seeded on all hydrogels during the whole study period compared to both controls. For G10_LNCO3, significantly higher values were measured at day six ($p<0.05$) and nine compared to G10_LNCO5 ($p<0.001$) and day two for G10_LNCO8 ($p<0.001$).

MCP-1 release by HUVEC was similar for the three hydrogels and glass two and six days after cell seeding. MCP-1 increased significantly in the cell culture supernatants of HUVEC seeded on G10_LNCO3 compared to G10_LNCO5, G10_LNCO8 and untreated control cells at day nine. This increase was comparable to HUVEC stimulated using IL-1β.

The concentration of IL-8 in the cell culture supernatants of HUVEC was similar for cultivation on the three hydrogels and glass during the whole study period. HUVEC stimulated with IL-1β released significantly higher amounts of IL-8 compared to the three hydrogels and glass at two, six and nine days of cultivation ($p<0.001$).

The following cytokines were only detected in supernatants of HUVEC stimulated with IL-1β: IL-6, IL-1β, IL-1Ra, TNF-α, RANTES, G-CSF, GM-CSF, MIP-1α, MIP-1β, eotaxin, and IP-10. FGF-basic was below the detection limit in all supernatants (see Table S1).

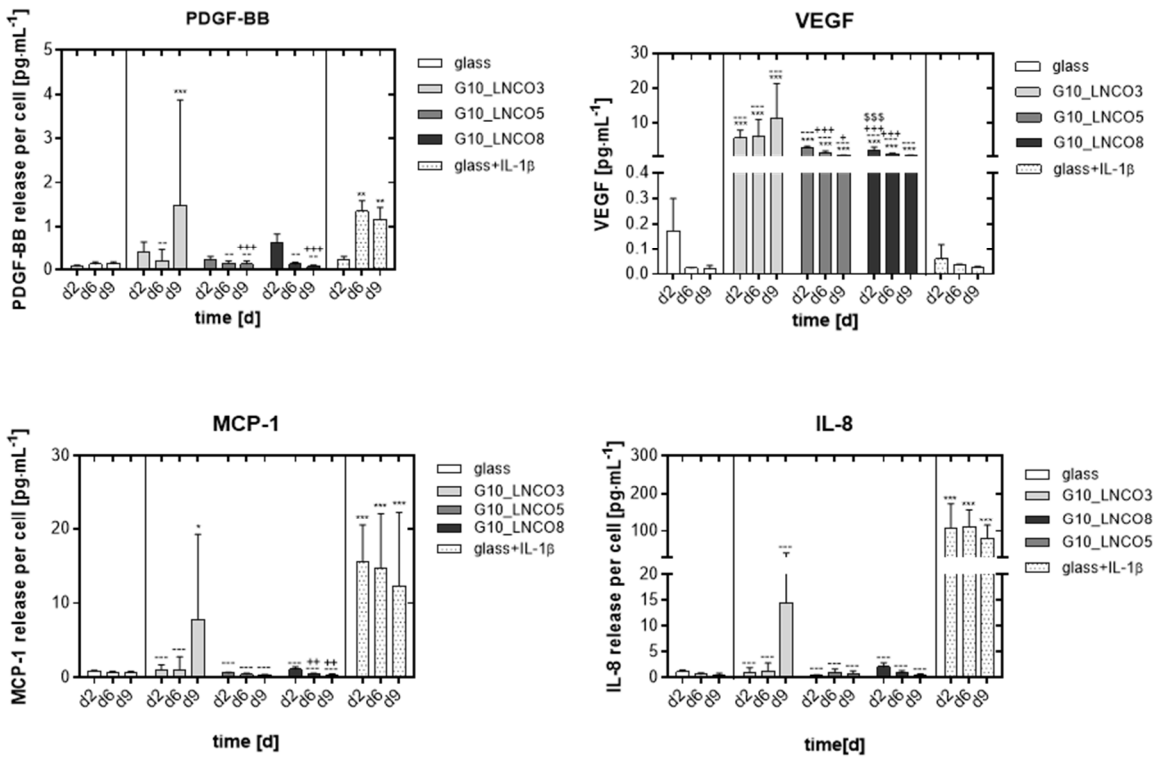

Figure 8: Concentrations of PDGF-BB, VEGF, MCP-1, and IL-8 in the cell culture supernatant of HUVEC seeded on the three hydrogels in comparison to glass as untreated control (UC) as well as to the IL-1β-treated control (ITC) after 2, 6 and 9 days of cell cultivation. Arithmetic mean ± SD of n=7 are presented. Statistical analysis was performed using Two-way Anova with Bonferroni post hoc test. .*: $p < 0.05$ versus glass .** : $p < 0.01$ versus glass, .*** : $p < 0.001$ versus glass, .++ : $p < 0.01$ versus G10_LNCO3, .+++ : $p < 0.001$ versus G10_LNCO3, $$$: $p < 0.001$ versus G10_LNCO5, --: $p < 0.01$ versus IL-1β, ---: $p < 0.001$ versus IL-1β

IV: Expression of pro-inflammatory markers

The expression of the pro-inflammatory proteins COX-1, COX-2 and RAGE in HUVEC was analyzed semi-quantitatively by Western blotting and densitometric analysis (Figure 9). Figure 9A shows representative images of the Western Blot analysis.

All three hydrogels induced differences in the expression of COX-1, COX-2, and RAGE in HUVEC (Figure 9B).

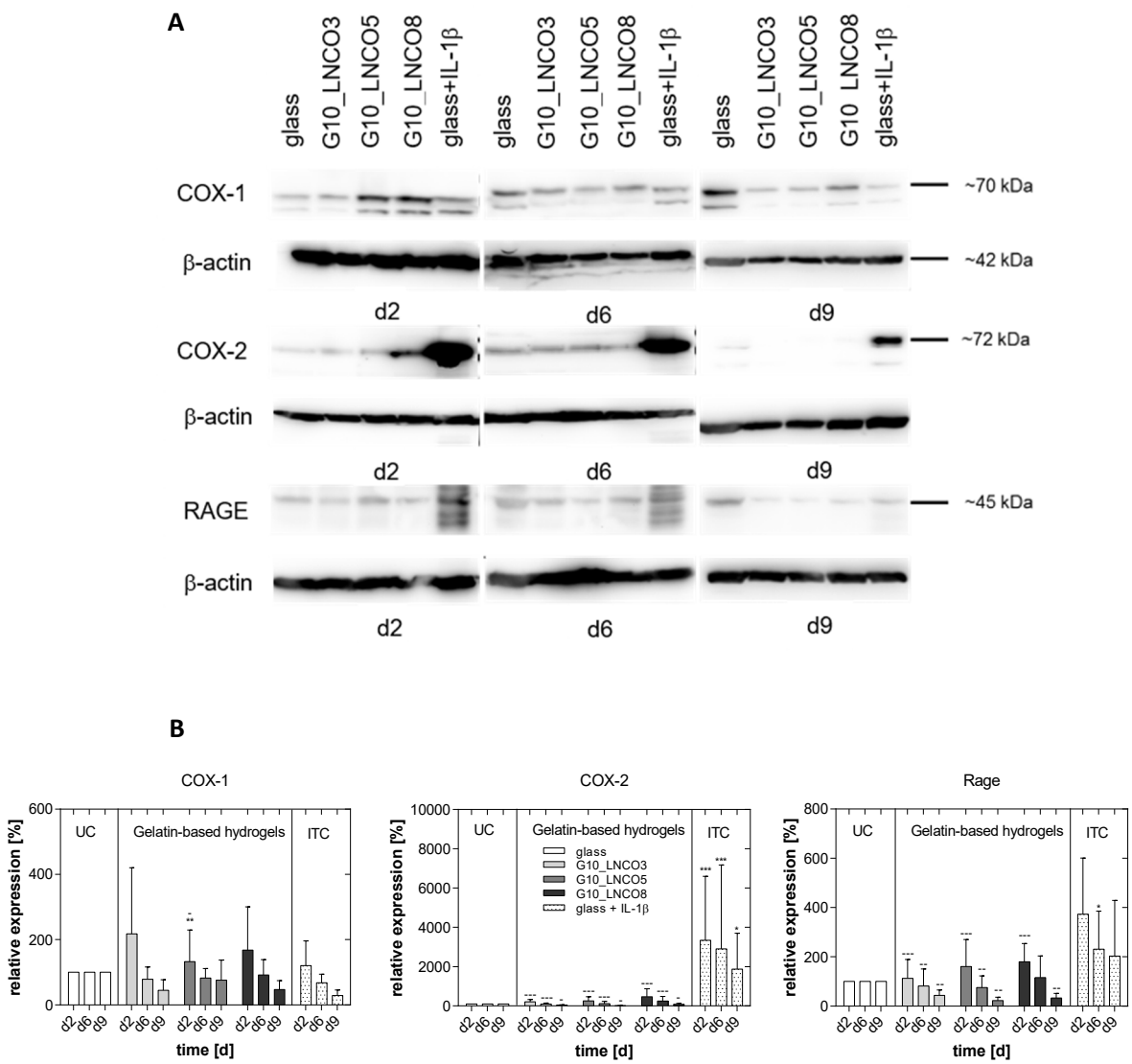

Figure 9. A) Representative images of the Western Blot analysis of COX-1, COX-2 and RAGE in HUVEC seeded on the three hydrogels in comparison to glass) as well as to the IL-1β-treated control after 2, 6 and 9 days of cell cultivation. B) Relative expression of inflammation-mediating proteins COX-1, COX-2 and RAGE in HUVEC seeded on the three hydrogels in comparison to glass as well as to the IL-1β-treated control after 2, 6 and 9 days of cell cultivation. Protein expression determined by Western blotting was related to the expression of β-actin using densitometric analysis. Arithmetic mean ± standard deviation of n=9 samples are presented. Statistical analysis was performed using Two-way ANOVA with Bonferroni post hoc test. *: $p < 0.05$ versus glass, **: $p < 0.01$ versus glass, ***: $p < 0.001$ versus glass, -: $p < 0.05$ versus IL-1β, ---: $p < 0.001$ versus IL-1β

The expression of COX-1 in HUVEC was comparable for all hydrogels during the whole study period ($p>0.05$ each) and comparable to the untreated control for G10_LNCO3 and G10_LNCO8. The expression of COX-2 in HUVEC seeded on the hydrogels did not differ from the untreated control during the whole study period, but was significantly lower than for the IL-1β-treated control ($p<0.001$). The expression of RAGE in HUVEC was significantly lower for the three hydrogels on day two and nine when compared to the IL-1β-treated control (d2: G10_LNCO3 vs glass+IL-1β: $p<0.001$, G10_LNCO5 vs glass+IL-1β $p<0.001$, G10_LNCO8 vs glass+IL-1β $p<0.001$, d9: G10_LNCO3, G10_LNCO5, G10_LNCO8 vs glass+IL-1β $p<0.01$). This applied – with the exception of G10_LNCO8 – also for day six; here, RAGE expression did not differ from the IL-1β-treated control.

DISCUSSION

The aim of the current study was to explore the adhesion, survival and function of human venous endothelial cells (HUVEC) on gelatin-based hydrogels. The understanding of the endothelialisation process will support the translation of the hydrogels in the venous system as e.g. left atrial appendage occluder or coating material for stents or vascular grafts.[46] Hence, morphology and viability of adherent HUVEC, the release response of the cells, pro-inflammatory markers, cell-to cell and cell-to-substrate contacts were investigated and related to the physicochemical properties of the hydrogel substrates.

By FT-IR spectroscopy, it was shown that there was a complete conversion of the isocyanate group of LDI used to stabilize the gelatin hydrogels. Any remaining isocyanate group otherwise might have led to toxic effects in contact with cells. As was suggested in earlier studies,[30] extended washing of the hydrogels is required to guarantee the conversion. FT-IR spectroscopy is furthermore suited to analyze protein conformations, especially by comparing amide I and amide II band positions and intensities. In case of gelatin and collagen, it was demonstrated that especially the amide I band is sensitive to temperature and has hence been associated with triple helix formation. In fact, in gelatin-based systems, the amide I band sometimes contains several peaks,[47-48] with a band at 1660 cm^{-1} representing the triple helical conformation. Especially in gelatins, there seems to be a continuous shift of the most intense

amide I band to higher wave numbers at lower temperatures, which may reflect partial folding. In addition, the amide II band is also observed at higher wavenumbers at lower temperatures / higher degree of folding. In the acquired spectra, no evidence for triple helical conformations was observed. This is in agreement with wide angle X-ray scattering of the discussed hydrogels.[29] It should be noted that the IR spectra were acquired from dried samples, and the drying regime might have prevented the formation of triple helices.[49] In that case, at lower temperatures in the equilibrium swollen samples some triple helicity might be present.

The contact angle, which mainly depends on the nature of the chemical groups on a surface as well as the surface roughness and quantifies the wettability of the surface, has been associated with the tendency for unspecific cell and protein adsorption,[50] and has reported to be an important criterion in the determination of the efficacy of implants in contact with blood.[51] Generally, it is understood that below an advancing contact angle of ~60-65° (Berg limit) water molecules cannot be replaced by hydrophobic groups of e.g. proteins and therefore unspecific adsorption is very limited. It can be argued that the nature of chemical groups on the surface of the studied hydrogels is very similar, as the materials are completely based on amino acids, and that therefore the surface roughness should have a larger influence on the wettability than the amount of LDI used in the synthesis. In fact, G10_LNCO5 had the highest roughness and the lowest contact angle of all three samples, though the relation between the two properties is not linear. However, neither the roughness nor the contact angle correlated with the adhesion of the endothelial cells. It should be noted that the relation of surface wettability and cell adhesion has been challenged as oversimplification.[52] One point is that the direct relation of contact angle and cell adhesion neglects the cells ability to sense their environment and respond with structural changes – they are not inert balls of predefined physicochemical properties. In the case studied here, it is likely that specific rather than unspecific interactions rule the cell adhesion, i.e. the peptidic cell adhesion sequences in the gelatin chains play a major role. In an earlier study, it was shown that plasma proteins such as fibrinogen may bind to gelatin hydrogels stabilized through reaction with LDI, and such protein adsorption might further influence the adhesion and proliferation of cells on the hydrogels.[53]

In contrast to wettability and surface roughness, both the macro- as well as the nanoscopic elasticity of the hydrogels increased continuously with increasing molar ratios of LDI in the starting material mixture, as was the case for the adherence of the endothelial cells. The netpoints of the hydrogels may consist of covalent bridges, interactions between grafted oligoureas and/or triple helical regions of the gelatin chains.[54] The rheological data were determined at 37 °C, while the AFM experiments were performed at ambient temperature. At ambient temperature, flexible segments of the gelatin might form triple helical regions, which as physical netpoints contribute to the mechanical resistance of the material to deformation. The general increase of G' and E_{red} has however to be attributed to bridging or grafted oligoureas, as the effect is also seen at 37 °C, and, as discussed above, neither FT-IR nor WAXS data suggest a strong tendency of the systems to form triple helices. The observed changes of mechanical properties correlate with earlier reported findings on the mechanical properties of such gelatin-based films determined in tensile tests at 37 °C on swollen samples in a water tank.[30] It should further be noted that the higher G‘ than G‘‘ values confirm that the hydrogels behave like a stabilized material rather than like a fluid.

The local elasticity - determined using the indentation method - measured the elasticity over an area comparable to a cell receptor size, covering altogether an area similar to one endothelial cell.[55] As the systems synthesized with higher amounts of LDI have a higher number of netpoints than the hydrogels synthesized with lower LDI equivalents, the density of gelatin chains in the material is also higher, which is reflected by the decrease of swelling with increasing amount of LDI used for the synthesis (Q = 1200±190 vol.-% (G10_LNCO3) and 360 ± 35 vol.-% (G10_LNCO8),[34] with the swelling of G10_LNCO5 being similar to G10_LNCO8[29]). This means that also the density of adhesion sites increased in the materials with increasing modulus. It can therefore be hypothesized that this effect contributed to the increased HUVEC attachment and proliferation on the G10_LNCO5 and G10_LNCO8 hydrogels compared to G10_LNCO3. A further aspect is the sensing of the micromechanical and biomechanical characteristics of the hydrogel surfaces by the HUVECs. As the exact location of adhesion sites is not known, these may have an influence on the overall attachment of a HUVEC cell layer but only a small effect on the individual

cell, which however will be influenced by the substrate's elasticity.[31, 56] The local elastic modulus, therefore, should have a significant influence on the response of HUVEC. It has been reported that HUVEC cell exhibited rounded morphologies on soft (E = 0.065±0.021 kPa) compared to more spread morphologies on harder (E = 1.032±0.083 kPa) hydrogel substrates, where the change in cell adherence due to mechanical stimuli is correlated to changes in the cytoskeletal actin fibers.[57] When culturing aortic endothelial cells on polyacrylamide gels of varying stiffnesses, there was an abrupt switch from round to spread morphologies and formation of stress fibres at G' values of ~3 kPa and higher.[58] ECM-derived substrates with higher Young's moduli (~10-17 kPa) have also been reported to successfully support the vascular morphogenesis of HUVEC, while a substrate with lower Young's modulus (5 kPa) failed to do so.[59] Thus, the elasticities of the hydrogels measured by rheology and AFM falls into the range (~1-10 kPa) in which changes of endothelial cell behaviour was noticed before. It can be hypothesized – and the results seem to confirm this hypothesis – that controlled by the elastic modulus, HUVEC release enzymes (essentially matrix metalloproteases), which subsequently change the entire microenvironment. The effect on matrix elasticity on cellular behaviour has been shown in quite diverse settings. For example, substrate elasticity pre-determined stem cell differentiation behavior,[31] and substrate elasticity was in all cases similar the elasticity of the tissues and matrices that are the typical environment of the cell lineages into which the stem cells differentiated. This also works in the 3D environment, in which osteogenesis could be guided by controlling the scaffolds mechanics in the range of E = 100-1000 kPa.[60] While there are several pathways for the mechanotransduction discussed, regulation of cytoskeletal tension leading to transcriptional activation seems an underlying principle.[61] While the basic rule has been thoroughly established, the exact conditions to promote a wanted function of a specific cell type remain to be elucidated step by step, partially as the determination of mechanical properties of living tissues is still challenging, the reported data may have been acquired with quite different setups and are therefore difficult to compare, there may be additional influences such as the presence of cell adhesions sites (or their absence), and due to the inherent variability between cells when not from the same donor or host.

In the remodelling phase the HUVEC secrete their own extracellular matrix and remain firmly bound to the ECM on the hydrogel during the degradation of the hydrogels. This is not possible for the soft hydrogel G10_LNCO3, so that for the fast degrading hydrogel many HUVEC remain in an activated and migrating state. A HUVEC monolayer did not develop on G10_LNCO3, probably because of the more rapid degradation in comparison to the other hydrogels. Former studies reported a mass loss of 40% for G10_LNCO3 after three days (G10_LNCO5: 30%, G10_LNCO8: 8%) (partly published in [34]). It is thought that during the faster degradation of G10_LNCO3 constantly linkages of single cellular focal adhesions are dissolved, so that a stable cell-to-substrate binding could not develop (in contrast to VE-cadherin which was comparable for all hydrogels and the control, Figure 5) and the HUVEC remained in a migrating state. Interestingly, the susceptibility of G10_LNCO3 to degradation went hand-in-hand with the release of MMPs further promoting the degradation of the matrix.

On glass surfaces (controls) an optically nearly confluent HUVEC monolayer had formed with a typical cobblestone pattern and physiological spread cells in close connection with each other nine days after seeding. This was also the case for HUVEC cultivated on the hydrogels with higher degree of crosslinking (G10_LNCO5, G10_LNCO8), while on G10_LNCO3 no confluent HUVEC monolayer developed. These results differ from those of a former study, which was performed with arterial endothelial cells over a cultivation time of 48 h in total [34] and, therefore, underline the differences between endothelial cells of different segments of the vascular tree. While the stress fibers remained constant on glass during the cultivation period, they decreased on G10_LNCO5 and G10_LNCO8 along with the formation of the marginal filament band, indicating an appropriate contact of the HUVEC to the cultivation substrates [62-63]. These results are in good agreement with the expression of the glycoprotein VE-Cadherin, which mediates cell-to-cell interactions, clustered in the HUVEC cell rims on the hydrogels, which was comparable with control cells during the nine days of cultivation. Schulz et al. could also show that HUVEC monolayers on G10_LNCO5 and on G10_LNCO8 were able to resist venous shear forces of 3 $dyn \cdot cm^{-2}$ over one hour, presenting a solid cell-to-substrate contact mediated by a strong interaction between VE-cadherin and the actin cytoskeleton of adjacent cells.[64]

On all hydrogels, islands without HUVEC were visible. These holes in the HUVEC monolayers were found in larger cavities at the surface of the hydrogels where no cells had grown into, while smaller cavities were filled out by HUVEC. These holes are a result of the processing during the material synthesis.

It was particularly striking that HUVEC on G10_LNCO3 remained in a spindle-shaped morphology presenting stress fibers until the ninth day of cultivation (comparable to IL-1β treated control HUVEC mimicking a pro-inflammatory driven situation) and a less significant marginal filament band typical of cell layers with a low cell-to-cell-binding. They appeared to be activated and were migrating over the whole cultivation period.

While the cell density and morphology of HUVEC clearly varied between the different hydrogels and the controls, the viability did not differ. The number of adherent viable cells on the three hydrogels was comparable to the control samples, while clearly less viable HUVEC were found in the IL-1β-treated control.

Matrix metalloproteases (MMPs) are involved in the degradation and remodeling of the extracellular matrix (ECM), which is mandatory for tissue regeneration.[65-66] Since the hydrogels are derived from collagen, they may partly mimic the structure of a native ECM and are, like the ECM, degraded by certain MMPs (e.g. by MMP2 or MMP9 [67]). Only in the supernatant of HUVEC seeded on G10_LNCO3 an increased MMP activity could be detected, which correlates well with the fast degradation of this hydrogel (compared to the two others). These results led to the assumption that the MMP activity was influenced by the relatively loose network of this hydrogel. Also, certain degradation products, or the lower elastic modulus might trigger the MMP activity, and – via mechanotransduction – may influence the rate of degradation.[68] On the other hand, the inhibition of the free diffusion of MMPs due to a higher number of covalent and physical netpoints in G10_LNCO5 and G10_LNCO8 might possibly contribute to a slower rate of degradation.

The metabolism of HUVEC in a pre-confluent status clearly differs from that after confluence.[41, 69-70] Therefore, the release behavior, an indicator of cellular function, was investigated at different time

points. The release of pro-inflammatory eicosanoids from HUVEC on hydrogels was similar to the release in control cultures after two days of cultivation.[71] The slight changes of the eicosanoids in the first week might be induced by the medium exchange every second day.[72] However, nine days after seeding, the highest release was observed for HUVEC cultivated on G10_LNCO3. This release was even higher than from HUVEC treated with pro-inflammatory IL-1β indicating that the cells on G10_LNCO3 were under stress, a status described as perturbation of endothelial cells.[73-75] In addition, the pre-confluent status of the cells, induced by the degradation of the material, could be another reason for this elevated release of eicosanoids.

The slightly increased release of TXA_2, PGI_2 and PGE_2 indicated a pro-inflammatory response of HUVEC on G10_LNCO3, confirmed by marginally increased amounts of pro-inflammatory cytokines like IL-8 and MCP-1 nine days after seeding. The expression of the pro-inflammatory marker COX-2, its constitutive isoform COX-1 and RAGE in HUVEC were only slightly, but not significantly elevated after cultivation on the hydrogels, also hinting to a very weak material-induced inflammation. In contrast, Ullm et al. reported that human arterial endothelial cells showed a crosslinking-dependent, increased expression of COX-2 after cultivation on G10_LNCO3 and G10_LNCO8.[34] These data demonstrate that the response of cells to biomaterials clearly differs between venous and arterial endothelial cells. Therefore, the *in vitro* evaluation of biomaterials should be performed with region-specific cells.[46, 76]

As described by Caughey et al., the synthesis of TXA_2 mostly depends on COX-1, whereas the synthesis of PGI_2 and PGE_2 relies on the activity of COX-2.[77] In line with this, neither the synthesis of COX-1 nor the release of TXA_2 was increased by HUVEC after cultivation with IL-1β. In contrast, IL-1β significantly enhanced the synthesis of COX-2 and subsequently the secretion of PGI_2 and PGE_2. Nevertheless, cultivation on G10_LNCO5 and G10_LNCO8 did not influence the release of eicosanoids by HUVEC, whereas G10_LNCO3, especially after 9 days of cultivation, induced a high secretion of eicosanoids, which even exceeded the effect of IL-1β. These results were also in line with the release of mediators of angiogenesis like PDGF-BB and VEGF, indicating a slight pro-inflammatory reaction which *in vivo* is of vital importance for the wound healing and the regenerative processes.[78-79]

These *in vitro* analyses demonstrate considerable differences in the behavior of HUVEC on the three hydrogels. Especially on G10_LNCO5 and G10_LNCO8 a functionally-confluent HUVEC monolayer developed presenting a release reaction comparable to control cells on glass. As these hydrogels degrade only slowly, their physicochemical characteristics and density of cell adhesion points are likely to play a predominant role in guiding the cellular behavior (see Figure 1). This indicates both hydrogels to be promising polymers for applications in the venous vascular system.

ACKNOWLEDGMENT

The authors thank the Helmholtz Association for funding of this work through program-oriented funding as well as through Helmholtz-Portfolio Topic “Technology and medicine”. A.K.G. was recipient of a fellowship of the Helmholtz Postdoc Program 2012 (PD-064). S.H. was recipient of a fellowship by Europäische Sozialfonds (ESF, 2012-2014). Technical assistance of Aline Morgenegg and Sebastian Meister (Dresden-Rossendorf) as well as of Jessica Reinert, Nicole Hüttig, and Peter Viszokai (Teltow) is greatly acknowledged.

SUPPORTING INFORMATION

Figure S1 Rheological behavior of the G10_LNCO3 (A), G10_LNCO5 (B), and G10_LNCO8 (C) hydrogels over time, Figure S2 Percentages of viable adherent HUVEC seeded on the three hydrogels in comparison to glass as well as to the IL-1β-treated control after 2, 6 and 9 days of cultivation, Figure S3 Viability staining of HUVEC after 9 days of cultivation, Table S1: Cytokines measured below the detection limit, measured only in the supernatant of inflammatory treated HUVEC and cytokines without biological activity.

REFERENCES

1. Zwaginga, J. J.; de Boer, H. C.; IJsseldijk, M.; Kerkhof, A.; Muller-Berghaus, G.; Gruhlichhenn, J.; Sixma, J. J.; de Groot, P. G., Thrombogenicity of vascular cells. Comparison between endothelial cells isolated from different sources and smooth muscle cells and fibroblasts. *Arterioscler., Thromb., Vasc. Biol.* **1990,** *10* (3), 437-448. DOI: 10.1161/01.atv.10.3.437
2. Jung, F.; Wischke, C.; Lendlein, A., Degradable, Multifunctional Cardiovascular Implants: Challenges and Hurdles. *MRS Bull.* **2011,** *35* (8), 607-613. DOI: 10.1557/mrs2010.529.
3. Pasquinelli, G.; Freyrie, A.; Preda, P.; Curti, T.; D'Addato, M.; Laschi, R., Healing of prosthetic arterial grafts. *Scanning Microsc.* **1990,** *4* (2), 351-362.
4. Park, J. W.; Gerk, U.; Franke, R. P.; Jung, F., Post-Mortem Analysis of a Left Atrial Appendage Occlusion Device (PLAATO™) in a Patient with Permanent Atrial Fibrillation. *Cardiology* **2009,** *112* (3), 205-208. DOI: 10.1159/000149574.
5. Park, J.-W.; Sherif, M. A.; Zintl, K.; Lam, Y.-Y.; Goedde, M.; Scharnweber, T.; Jung, F.; Franke, R. P.; Brachmann, J., Percutaneous left atrial appendage closure with a novel self-modelizing device: A pre-clinical feasibility study. *Int. J. Cardiol.* **2014,** *177* (3), 957-963. DOI: 10.1016/j.ijcard.2014.09.194.
6. Zilla, P.; Bezuidenhout, D.; Human, P., Prosthetic vascular grafts: Wrong models, wrong questions and no healing. *Biomaterials* **2007,** *28* (34), 5009-5027. DOI: 10.1016/j.biomaterials.2007.07.017.
7. Sarkar, S.; Salacinski, H. J.; Hamilton, G.; Seifalian, A. M., The Mechanical Properties of Infrainguinal Vascular Bypass Grafts: Their Role in Influencing Patency. *Europ. J. Vasc. Edovasc. Surg.* **2006,** *31* (6), 627-636. DOI: 10.1016/j.ejvs.2006.01.006.
8. Varga, M.; Matia, I.; Lodererova, A.; Adamec, M., The minimal dose of FK506 is sufficient to facilitate the arterialisation of venous allografts in rats. *Europ. Surg.* **2013,** *45* (1), 8-14. DOI: 10.1007/s10353-012-0179-3.
9. Reinhart-King, C. A.; Dembo, M.; Hammer, D. A., The Dynamics and Mechanics of Endothelial Cell Spreading. *Biophys. J.* **2005,** *89* (1), 676-689. DOI: 10.1529/biophysj.104.054320.
10. Feugier, P.; Black, R. A.; Hunt, J. A.; How, T. V., Attachment, morphology and adherence of human endothelial cells to vascular prosthesis materials under the action of shear stress. *Biomaterials* **2005,** *26* (13), 1457-1466. DOI: 10.1016/j.biomaterials.2004.04.050.
11. Raimbault, O.; Benayoun, S.; Anselme, K.; Mauclair, C.; Bourgade, T.; Kietzig, A.-M.; Girard-Lauriault, P.-L.; Valette, S.; Donnet, C., The effects of femtosecond laser-textured Ti-6Al-4V on wettability and cell response. *Mater. Sci. Eng., C* **2016,** *69*, 311-320. DOI: 10.1016/j.msec.2016.06.072.
12. Potthoff, E.; Franco, D.; D'Alessandro, V.; Starck, C.; Falk, V.; Zambelli, T.; Vorholt, J. A.; Poulikakos, D.; Ferrari, A., Toward a Rational Design of Surface Textures Promoting Endothelialization. *Nano Lett.* **2014,** *14* (2), 1069-1079. DOI: 10.1021/nl4047398.
13. Shen, Y.; Ma, Y.; Gao, M.; Lai, Y.; Wang, G.; Yu, Q.; Cui, F.-z.; Liu, X., Integrins-FAK-Rho GTPases Pathway in Endothelial Cells Sense and Response to Surface Wettability of Plasma Nanocoatings. *ACS Appl. Mater. Interfaces* **2013,** *5* (11), 5112-5121. DOI: 10.1021/am400973a.
14. Aminian, A.; Shirzadi, B.; Azizi, Z.; Maedler, K.; Volkmann, E.; Hildebrand, N.; Maas, M.; Treccani, L.; Rezwan, K., Enhanced cell adhesion on bioinert ceramics mediated by the osteogenic cell membrane enzyme alkaline phosphatase. *Mater. Sci. Eng., C* **2016,** *69*, 184-194. DOI: 10.1016/j.msec.2016.06.056.
15. Oyen, M. L., Mechanical characterisation of hydrogel materials. *Int. Mater. Rev.* **2014,** *59* (1), 44-59. DOI: 10.1179/1743280413Y.0000000022.
16. Shen, Y.; Gao, M.; Ma, Y.; Yu, H.; Cui, F.-z.; Gregersen, H.; Yu, Q.; Wang, G.; Liu, X., Effect of surface chemistry on the integrin induced pathway in regulating vascular endothelial cells migration. *Colloids Surf., B* **2015,** *126*, 188-197. DOI: 10.1016/j.colsurfb.2014.12.019.

17. Pratt, K. J.; Jarrell, B. E.; Williams, S. K.; Carabasi, R. A.; Rupnick, M. A.; Hubbard, F. A., Kinetics of endothelial cell-surface attachment forces. *J. Cardiovasc. Surg.* **1988,** *7* (4), 591-599. DOI: 10.1016/0741-5214(88)90366-7.
18. Williams, S. K.; Jarrell, B. E.; Friend, L.; Radomski, J. S.; Carabasi, R. A.; Koolpe, E.; Mueller, S. N.; Thornton, S. C.; Marinucci, T.; Levine, E., Adult human endothelial cell compatibility with prosthetic graft material. *J. Surg. Res.* **1985,** *38* (6), 618-629. DOI: 10.1016/0022-4804(85)90084-8.
19. Furth, M. E.; Atala, A.; Van Dyke, M. E., Smart biomaterials design for tissue engineering and regenerative medicine. *Biomaterials* **2007,** *28* (34), 5068-5073. DOI: 10.1016/j.biomaterials.2007.07.042.
20. Kang, D.; Kim, J. H.; Jeong, Y. H.; Kwak, J.-Y.; Yoon, S.; Jin, S., Endothelial monolayers on collagen-coated nanofibrous membranes: cell–cell and cell–ECM interactions. *Biofabrication* **2016,** *8* (2), 025008. DOI: 10.1088/1758-5090/8/2/025008.
21. Neffe, A. T.; von Ruesten-Lange, M.; Braune, S.; Lützow, K.; Roch, T.; Richau, K.; Krüger, A.; Becherer, T.; Thünemann, A. F.; Jung, F., Multivalent grafting of hyperbranched oligo-and polyglycerols shielding rough membranes to mediate hemocompatibility. *Journal of Materials Chemistry B* **2014,** *2* (23), 3626-3635.
22. Kushwaha, M.; Anderson, J. M.; Bosworth, C. A.; Andukuri, A.; Minor, W. P.; Lancaster, J. R.; Anderson, P. G.; Brott, B. C.; Jun, H.-W., A nitric oxide releasing, self assembled peptide amphiphile matrix that mimics native endothelium for coating implantable cardiovascular devices. *Biomaterials* **2010,** *31* (7), 1502-1508. DOI: 10.1016/j.biomaterials.2009.10.051.
23. Davidenko, N.; Schuster, C. F.; Bax, D. V.; Farndale, R. W.; Hamaia, S.; Best, S. M.; Cameron, R. E., Evaluation of cell binding to collagen and gelatin: a study of the effect of 2D and 3D architecture and surface chemistry. *J. Mater. Sci.: Mater. Med.* **2016,** *27* (10), 1-14. DOI: 10.1007/s10856-016-5763-9.
24. Burdick, J. A.; Mauck, R. L.; Gorman, J. H.; Gorman, R. C., Acellular biomaterials: an evolving alternative to cell-based therapies. *Sci. Transl. Med.* **2013,** *5* (176), 176ps4.
25. Vekilov, D. P.; Grande-Allen, K. J., Mechanical Properties of Diseased Veins. *Methodist Debakey Cardiovasc J* **2018,** *14* (3), 182-187. DOI: 10.14797/mdcj-14-3-182.
26. Broekema, F. I.; van Oeveren, W.; Boerendonk, A.; Sharma, P. K.; Bos, R. R., Hemostatic action of polyurethane foam with 55% polyethylene glycol compared to collagen and gelatin. *Bio-Med. Mater. Eng.* **2016,** *27* (2-3), 149-159. DOI: 10.3233/BME-161578.
27. Delgado, L. M.; Bayon, Y.; Pandit, A.; Zeugolis, D. I., To cross-link or not to cross-link? Cross-linking associated foreign body response of collagen-based devices. *Tissue Eng., Part B* **2015,** *21* (3), 298-313. DOI: 10.1089/ten.teb.2014.0290.
28. Löwenberg, C.; Tripodo, G.; Julich-Gruner, K. K.; Neffe, A. T.; Lendlein, A., Supramolecular Gelatin Networks Based on Inclusion Complexes. *Macromolecular Bioscience* **2020**, 2000221.
29. Tronci, G.; Neffe, A. T.; Pierce, B. F.; Lendlein, A., An entropy-elastic gelatin-based hydrogel system. *Journal of Materials Chemistry* **2010,** *20* (40), 8875-8884. DOI: 10.1039/C0JM00883D.
30. Neffe, A. T.; Gebauer, T.; Lendlein, A., Tailoring of mechanical properties of diisocyanate crosslinked gelatin-based hydrogels. *Mater. Res. Soc. Symp. Proc.* **2013,** *1569*, 3-8. DOI: 10.1557/opl.2013.831.
31. Engler, A. J.; Sen, S.; Sweeney, H. L.; Discher, D. E., Matrix elasticity directs stem cell lineage specification. *Cell* **2006,** *126* (4), 677-689.
32. Pierce, B. F.; Pittermann, E.; Ma, N.; Gebauer, T. P.; Neffe, A. T.; Hölscher, M.; Jung, F.; Lendlein, A., Viability of Human Mesenchymal Stem Cells Seeded on Crosslinked Entropy-Elastic Gelatin-Based Hydrogels. *Macromolecular Bioscience* **2012,** *12* (3), 312-321. DOI: 10.1002/mabi.201100237.
33. Rijckaert, B.; Neffe, A. T.; Roch, T.; Gebauer, T. P.; Pierce, B. F.; Görs, J.; Smink, J. J.; Gossen, M.; Lendlein, A.; Leutz, A., A High Content Screening Assay for Evaluation of Biomaterial-Mediated Cell Fusion Processes. *Macromolecular Symposia* **2014,** *346* (1), 91-99. DOI: 10.1002/masy.201400147.

34. Ullm, S.; Krüger, A.; Tondera, C.; Gebauer, T. P.; Neffe, A. T.; Lendlein, A.; Jung, F.; Pietzsch, J., Biocompatibility and inflammatory response in vitro and in vivo to gelatin-based biomaterials with tailorable elastic properties. *Biomaterials* **2014,** *35* (37), 9755-66. DOI: 10.1016/j.biomaterials.2014.08.023.
35. Tondera, C.; Hauser, S.; Krüger-Genge, A.; Jung, F.; Neffe, A. T.; Lendlein, A.; Klopfleisch, R.; Steinbach, J.; Neuber, C.; Pietzsch, J., Gelatin-based Hydrogel Degradation and Tissue Interaction in vivo: Insights from Multimodal Preclinical Imaging in Immunocompetent Nude Mice. *Theranostics* **2016,** *6* (12), 2114-2128. DOI: 10.7150/thno.16614.
36. Aird, W. C., Endothelial cell heterogeneity. *Crit. Care Med.* **2003,** *31* (4), S221-S230. DOI: 10.1097/01.ccm.0000057847.32590.c1.
37. Bubnis, W. A.; Ofner, C. M., The determination of ϵ-amino groups in soluble and poorly soluble proteinaceous materials by a spectrophotometrie method using trinitrobenzenesulfonic acid. *Anal. Biochem.* **1992,** *207* (1), 129-133. DOI: 10.1016/0003-2697(92)90513-7.
38. Welzel, P. B.; Prokoph, S.; Zieris, A.; Grimmer, M.; Zschoche, S.; Freudenberg, U.; Werner, C., Modulating Biofunctional starPEG Heparin Hydrogels by Varying Size and Ratio of the Constituents. *Polymers* **2011,** *3* (1), 602. DOI: 10.3390/polym3010602.
39. Franke, R.-P.; Fuhrmann, R.; Hiebl, B.; Jung, F., Influence of various radiographic contrast media on the buckling of endothelial cells. *Microvasc. Res.* **2008,** *76* (2), 110-113. DOI: 10.1016/j.mvr.2008.05.002.
40. Krüger, A.; Fuhrmann, R.; Jung, F.; Franke, R. P., Influence of the coating with extracellular matrix and the number of cell passages on the endothelialization of a polystyrene surface. *Clin. Hemorheol. Microcirc.* **2015,** *60* (1), 153-61. DOI: 10.3233/CH-151943.
41. Krüger, A.; Mayer, A.; Roch, T.; Schulz, C.; Lendlein, A.; Jung, F., Angiogenically stimulated alternative monocytes maintain their pro-angiogenic and non-inflammatory phenotype in long-term co-cultures with HUVEC. *Clin. Hemorheol. Microcirc.* **2014,** *58* (1), 229-240. DOI: 10.3233/CH-141875
42. Roch, T.; Akymenko, O.; Krüger, A.; Jung, F.; Ma, N.; Lendlein, A., Expression pattern analysis and activity determination of matrix metalloproteinase derived from human macrophage subsets. *Clin. Hemorheol. Microcirc.* **2014,** *58* (1), 147-58. DOI: 10.3233/CH-141885.
43. Wolf, S.; Haase-Kohn, C.; Lenk, J.; Hoppmann, S.; Bergmann, R.; Steinbach, J.; Pietzsch, J., Expression, purification and fluorine-18 radiolabeling of recombinant S100A4: a potential probe for molecular imaging of receptor for advanced glycation endproducts in vivo? *Amino Acids* **2011,** *41* (4), 809-820. DOI: 10.1007/s00726-010-0822-x.
44. Yap, A. S.; Kovacs, E. M., Direct cadherin-activated cell signaling: a view from the plasma membrane. *J. Cell. Biol.* **2003,** *160* (1), 11-6. DOI: 10.1083/jcb.200208156.
45. Huveneers, S.; Danen, E. H., Adhesion signaling–crosstalk between integrins, Src and Rho. *J. Cell Sci.* **2009,** *122* (8), 1059-1069. DOI: 10.1242/jcs.039446
46. Hauser, S.; Jung, F.; Pietzsch, J., Human Endothelial Cell Models in Biomaterial Research. *Trends Biotechnol.* **2017,** *35* (3), 265-277. DOI: 10.1016/j.tibtech.2016.09.007.
47. Payne, K.; Veis, A., Fourier transform IR spectroscopy of collagen and gelatin solutions: deconvolution of the amide I band for conformational studies. *Biopolymers: Original Research on Biomolecules* **1988,** *27* (11), 1749-1760.
48. Prystupa, D.; Donald, A., Infrared study of gelatin conformations in the gel and sol states. *Polymer Gels and Networks* **1996,** *4* (2), 87-110.
49. Zaupa, A.; Neffe, A. T.; Pierce, B. F.; Nochel, U.; Lendlein, A., Influence of Tyrosine-Derived Moieties and Drying Conditions on the Formation of Helices in Gelatin. *Biomacromolecules* **2011,** *12* (1), 75-81. DOI: 10.1021/bm101029k.
50. Schilp, S.; Kueller, A.; Rosenhahn, A.; Grunze, M.; Pettitt, M. E.; Callow, M. E.; Callow, J. A., Settlement and adhesion of algal cells to hexa (ethylene glycol)-containing self-assembled monolayers with systematically changed wetting properties. *Biointerphases* **2007,** *2* (4), 143-150.
51. Williams, D. F., On the mechanisms of biocompatibility. *Biomaterials* **2008,** *29* (20), 2941-2953. DOI: 10.1016/j.biomaterials.2008.04.023.

52. Alexander, M. R.; Williams, P., Water contact angle is not a good predictor of biological responses to materials. *Biointerphases* **2017,** *12* (2), 02C201. DOI: 10.1116/1.4989843.
53. Schönwälder, S. M. S.; Bally, F.; Heinke, L.; Azucena, C.; Bulut, O. z. l. D.; Heißler, S.; Kirschhöfer, F.; Gebauer, T. P.; Neffe, A. T.; Lendlein, A.; Brenner-Weiß, G.; Lahann, J.; Welle, A.; Overhage, J.; Wöll, C., Interaction of human plasma proteins with thin gelatin-based hydrogel films: a QCM-D and ToF-SIMS study. *Biomacromolecules* **2014,** *15* (7), 2398-406. DOI: 10.1021/bm500750v.
54. Neffe, A. T.; Pierce, B. F.; Tronci, G.; Ma, N.; Pittermann, E.; Gebauer, T.; Frank, O.; Schossig, M.; Xu, X.; Willie, B. M.; Forner, M.; Ellinghaus, A.; Lienau, J.; Duda, G. N.; Lendlein, A., One step creation of multifunctional 3D architectured hydrogels inducing bone regeneration. *Adv. Mater.* **2015,** *27* (10), 1738-44. DOI: 10.1002/adma.201404787.
55. Buxboim, A.; Ivanovska, I. L.; Discher, D. E., Matrix elasticity, cytoskeletal forces and physics of the nucleus: how deeply do cells 'feel' outside and in? *J. Cell Sci.* **2010,** *123* (3), 297-308. DOI: 10.1242/jcs.041186.
56. Müller, C.; Pompe, T., Distinct impacts of substrate elasticity and ligand affinity on traction force evolution. *Soft Matter* **2016,** *12* (1), 272-280.
57. Jalali, S.; Tafazzoli-Shadpour, M.; Haghighipour, N.; Omidvar, R.; Safshekan, F., Regulation of endothelial cell adherence and elastic modulus by substrate stiffness. *Cell communication & adhesion* **2015,** *22* (2-6), 79-89.
58. Yeung, T.; Georges, P. C.; Flanagan, L. A.; Marg, B.; Ortiz, M.; Funaki, M.; Zahir, N.; Ming, W.; Weaver, V.; Janmey, P. A., Effects of substrate stiffness on cell morphology, cytoskeletal structure, and adhesion. *Cell motility and the cytoskeleton* **2005,** *60* (1), 24-34.
59. Du, P.; Subbiah, R.; Park, J.-H.; Park, K., Vascular morphogenesis of human umbilical vein endothelial cells on cell-derived macromolecular matrix microenvironment. *Tissue Engineering Part A* **2014,** *20* (17-18), 2365-2377.
60. Chatterjee, K.; Lin-Gibson, S.; Wallace, W. E.; Parekh, S. H.; Lee, Y. J.; Cicerone, M. T.; Young, M. F.; Simon Jr, C. G., The effect of 3D hydrogel scaffold modulus on osteoblast differentiation and mineralization revealed by combinatorial screening. *Biomaterials* **2010,** *31* (19), 5051-5062.
61. Yang, C.; DelRio, F. W.; Ma, H.; Killaars, A. R.; Basta, L. P.; Kyburz, K. A.; Anseth, K. S., Spatially patterned matrix elasticity directs stem cell fate. *Proceedings of the National Academy of Sciences* **2016,** *113* (31), E4439-E4445.
62. Drenckhahn, D., Cell motility and cytoplasmic filaments in vascular endothelium. In *Structure and Function of Endothelial Cells*, Karger Publishers: 1983; pp 53-70.
63. Franke, R.; Gräfe, M.; Dauer, U.; Schnittler, H.; Mittermayer, C., Stress fibres (SF) in human endothelial cells (HEC) under shear stress. *Klin. Wochenschr.* **1986,** *64* (19), 989-992.
64. Schulz, C.; Vukicevic, R.; Krüger-Genge, A.; Neffe, A. T.; Lendlein, A.; Jung, F., Monolayer formation and shear- resistance of human vein endothelial cells on gelatin-based hydrogels with tailorable elasticity and degradability. *Clin. Hemorheol. Microcirc.* **2016,** *64* (4), 699-710. DOI: 10.3233/CH-168007.
65. Rother, S.; Samsonov, S. A.; Hofmann, T.; Blaszkiewicz, J.; Köhling, S.; Moeller, S.; Schnabelrauch, M.; Rademann, J.; Kalkhof, S.; von Bergen, M., Structural and functional insights into the interaction of sulfated glycosaminoglycans with tissue inhibitor of metalloproteinase-3–A possible regulatory role on extracellular matrix homeostasis. *Acta Biomater.* **2016,** *45*, 143-154. DOI: 10.1016/j.actbio.2016.08.030
66. Voepel, J.; Edlund, U.; Albertsson, A. C.; Percec, V., Hemicellulose-Based Multifunctional Macroinitiator for Single-Electron-Transfer Mediated Living Radical Polymerization. *Biomacromolecules* **2011,** *12*, 253-259.
67. Werb, Z., ECM and Cell Surface Proteolysis: Regulating Cellular Ecology. *Cell* **1997,** *91* (4), 439-442. DOI: 10.1016/S0092-8674(00)80429-8.
68. Coon, B. G.; Baeyens, N.; Han, J.; Budatha, M.; Ross, T. D.; Fang, J. S.; Yun, S.; Thomas, J.-L.; Schwartz, M. A., Intramembrane binding of VE-cadherin to VEGFR2 and VEGFR3 assembles the

endothelial mechanosensory complex. *J. Cell. Biol.* **2015,** *208* (7), 975-986. DOI: 10.1083/jcb.201408103.
69. Mayer, A.; Roch, T.; Kratz, K.; Lendlein, A.; Jung, F., Pro-angiogenic CD14++ CD16+ CD163+ monocytes accelerate the in vitro endothelialization of soft hydrophobic poly (n-butyl acrylate) networks. *Acta Biomaterialia* **2012,** *8* (12), 4253-4259.
70. De Caterina, R.; Dorso, C. R.; Tack-Goldman, K.; Weksler, B. B., Nitrates and endothelial prostacyclin production: studies in vitro. *Circulation* **1985,** *71* (1), 176-182. DOI: 10.1161/01.CIR.71.1.176.
71. Birukova, A. A.; Zagranichnaya, T.; Fu, P.; Alekseeva, E.; Chen, W.; Jacobson, J. R.; Birukov, K. G., Prostaglandins PGE_2 and PGI_2 promote endothelial barrier enhancement via PKA-and Epac1/Rap1-dependent Rac activation. *Exp. Cell Res.* **2007,** *313* (11), 2504-2520. DOI: 10.1016/j.yexcr.2007.03.036.
72. Krüger-Genge, A.; Fuhrmann, R.; Jung, F.; Franke, R., Morphology of primary human venous endothelial cell cultures before and after culture medium exchange. *Clin. Hemorheol. Microcirc.* **2015,** *61* (2), 151-156. DOI: 10.3233/CH-151992.
73. Brox, J. H.; Nordøy, A., Prostacyclin and ^{51}Cr release in cultured human endothelial cells. *Pathophysiol. Haemostasis Thromb.* **1982,** *12* (4), 345-352. DOI: 10.1159/000214692.
74. Holland, J.; Pritchard, K.; Rogers, N.; Stemerman, M., Perturbation of cultured human endothelial cells by atherogenic levels of low density lipoprotein. *Am. J. Pathol.* **1988,** *132* (3), 474.
75. Mitchell, J. A.; Ali, F.; Bailey, L.; Moreno, L.; Harrington, L. S., Role of nitric oxide and prostacyclin as vasoactive hormones released by the endothelium. *Exp. Physiol.* **2008,** *93* (1), 141-147. DOI: 10.1113/expphysiol.2007.038588.
76. Lazo, J. S., Endothelial injury caused by antineoplastic agents. *Biochem. Pharmacol.* **1986,** *35* (12), 1919-1923. DOI: 10.1016/0006-2952(86)90720-3.
77. Caughey, G. E.; Cleland, L. G.; Gamble, J. R.; James, M. J., Up-regulation of Endothelial Cyclooxygenase-2 and Prostanoid Synthesis by Platelets. Role of Thromboxane A2. *J. Biol. Chem.* **2001,** *276* (41), 37839-37845. DOI: 10.1074/jbc.M010606200.
78. Dreesmann, L.; Ahlers, M.; Schlosshauer, B., The pro-angiogenic characteristics of a cross-linked gelatin matrix. *Biomaterials* **2007,** *28* (36), 5536-5543. DOI: 10.1016/j.biomaterials.2007.08.040.
79. Jung, S.; Kleinheinz, J., Angiogenesis: the key to regeneration. *Regener. Med. Tissue Eng.* **2013**, 453-473. DOI: 10.5772/55542.

For Table of Contents Use only

Response of endothelial cells to gelatin-based hydrogels

Anne Krüger-Genge, Sandra Hauser, Axel T. Neffe, Yue Liu, Andreas Lendlein*, Jens Pietzsch, Friedrich Jung*